JOURNAL OF PROPULSION AND POWER
Vol. 30, No. 6, November–December 2014

Quasi-One-Dimensional Multimodes Analysis for Dual-Mode Scramjet

Lu Tian,* Lihong Chen,† Qiang Chen,‡ Fei Li,§ and Xinyu Chang¶
State Key Laboratory of High-Temperature Gas Dynamics, Chinese Academy of Sciences, 100190 Beijing, People's Republic of China

DOI: 10.2514/1.B35177

A quasi-one-dimensional analytical method with a novel model for precombustion shock train has been proposed to model different modes in the dual-mode scramjet flowfield. The interaction between shock and combustion is modeled by a strength-adaptable model in the isolator, named the "X shock." An iterative procedure is implemented to solve the precombustion shock and the flow properties downstream. The calculation of the combustor is based on a series of governing equations where the effects of area change, friction, and mass injection are included. The release of energy is obtained from a fuel-mixing model or pregiven heat release distributions estimated from experimental results. The numerical results of pressure are compared with the experimental data for validation of the present model. The results show that the quasi-one-dimesional method can be applied to analyze diverse modes in the whole process of the dual-mode scramjet combustor.

Nomenclature

A	=	geometric area of the duct, m^2
D	=	hydraulic diameter, m
h	=	mean specific enthalpy of a mixture, kJ/kg
h_i	=	specific enthalpy of the ith species, kJ/kg
M	=	Mach number
$\dot{m}$	=	mass flow rate, kg/s
p	=	pressure, Pa
s	=	specific entropy J/(kg · K)
T	=	temperature, K
U	=	velocity along the duct, m/s
ρ	=	density, kg/m^3

Subscripts

in	=	conditions in the inlet of the isolator
max	=	maximum value
min	=	minimum value
0	=	total or stagnation conditions

I. Introduction

THE hypersonic vehicle has been developed rapidly with successful flight tests [1,2].** The further requirement of the propulsion system is the robustness that the engine can operate efficiently and reliably along the flight path. The dual-mode scramjet engine, proposed in [3], has raised the interest of researchers all over the world. As shown in Fig. 1 [4], the dual-mode scramjet, which adopts the ramjet mode with the flight Mach number range of three to six and the scramjet mode with higher flight Mach number, could offer better performance. However, complex phenomena, such as precombustion shock train, the establishment of the thermal throat, and the strong interaction between the shock system and turbulence, are coupled in the dual-mode systems and bring difficulties in both experimental and computational studies. Besides, full-fidelity modeling is computationally expensive. Thus, a relatively accurate and efficient analytical procedure that can account for the whole process of the dual-mode scramjet is preferred.

To clarify the ability and limitation of the analytical method, different modes that might happen in the whole process of the dual-mode scramjet should be defined. As shown in Fig. 2, the dual-mode scramjet engine consists of inlet, isolator, combustor, and nozzle. The isolator connecting inlet and combustor prevents the shock structure caused by high pressure in the combustor propagate upstream. To distinguish different modes in the dual-mode scramjet, four modes were defined according to the state in the isolator and combustion downstream. When there are only very weak shock structures in the isolator and the averaged Mach number is above one along the whole engine duct, the mode is called "supersonic combustion mode," as shown in Fig. 2a. Because of less heat release, the shock structure is too weak to cause significant pressure rise upstream of the injection. On the contrary, when a large amount of heat release occurs in the combustor, very strong shock structures, such as a normal shock, could appear in the isolator and even cause unstart of the engine. When the averaged Mach number in the combustor is below one, the mode is defined as "subsonic combustion mode," as shown in Fig. 2d. More commonly, an obvious shock train system with different intensity would appear in the isolator of the dual-mode combustion configuration. Thus, "dual-mode supersonic combustion mode" and "dual-mode subsonic combustion mode" are distinguished by the averaged Mach number in the combustor, as shown in Figs. 2b and 2c. The main characteristics of the flowfield are so different that the four modes are defined to explain the abilities of the analytical methods and verify the analytical strategy.

For the analysis of scramjet engine performance, quasi-one-dimensional modeling has been widely used due to its high efficiency and convenience [5–13]. These models can be categorized into two groups according to the assumption of the flow. If the flow is assumed at the steady state, a series of ordinary differential equations (ODEs) are used. Otherwise, quasi-one-dimensional Euler equations are implemented for unsteady models. By implementing the ODEs [5–9], a relatively continuous flowfield can be calculated; without considering discontinuity caused by the shock structure in the isolator, only certain modes approaching supersonic combustion mode can be analyzed precisely. On the other hand, the unsteady quasi-one-dimensional (quasi-1-D) model [10–13] can automatically track the position of shock discontinuity; but as shown in Fig. 3 [13], a sudden jump appears in the isolator that behaves like a normal shock.

Received 17 September 2013; revision received 27 December 2013; accepted for publication 3 January 2014; published online 22 April 2014.

*Graduate Student, Institute of Mechanics; tianlu@imech.ac.cn.
†Professor, Institute of Mechanics; lhchen@imech.ac.cn. Senior Member AIAA.
‡Assistant Professor, Institute of Mechanics; chenqiang@imech.ac.cn.
§Associate Professor, Institute of Mechanics; lifei@imech.ac.cn.
¶Professor, Institute of Mechanics; xychang@imech.ac.cn. Senior Member AIAA.

**Data available online at http://en.wikipedia.org/wiki/Boeing_X-51 [retrieved 26 May 2010].

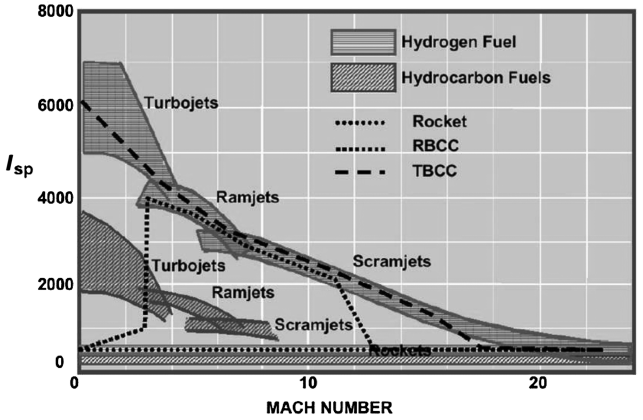

Fig. 1 Specific impulse of different engines with respect to flight Mach number [4] (RBCC-Rocket-Based Combined Cycle; TBCC-Turbine Based Combined Cycle).

In fact, the strength of shock systems in the dual-mode scramjet is usually weaker than that of a normal shock. Thus, dual-mode subsonic combustion mode cannot be analyzed accurately even if employing an unsteady model.

To sum up, lack of a strength-adaptable shock model in the isolator makes the previous 1-D models inapplicable for analyzing the whole process of the dual-mode scramjet. Besides, an interactive process is also required to simulate the interaction between shock and combustion in the dual-mode scramjet.

Thus, the aim of the present work is to put forward a multimode analytical method with the strength-adaptable shock model and interactive analytical procedure for the dual-mode scramjet. Although two-dimensional (2-D) and three dimensional analytical approaches can certainly capture the relevant shock structures and combustion behavior of the engine, they can be computationally expensive and inapplicable to preliminary design when a number of cases are required. On the other hand, the quasi-one-dimensional approach proposed next, reflecting the basic characteristics of shock trains and the interaction with combustion, can be done in seconds and further used in preliminary design of the dual-mode scramjet.

II. Methodology

As mentioned in the Sec. I, a strength-adaptable isolator model is needed to accomplish a multimodes analytical method for the dual-mode scramjet. However, it is difficult to introduce the pure 1-D equations to simulate the complex interaction between shock and combustion. Therefore, the flow is treated as three parts: the upstream is a 2-D shock structure to balance the shock and combustion interaction, the downstream is 1-D continuous flow with heat release to simulate combustion, and the transition of 2-D parameters to 1-D is made based on the conservation equations. First, a two-dimensional shock structure is induced to model the shock train. As shown in Fig. 4, a reflected shock-pair model named X shock has been established to calculate discontinuity caused by the precombustion shock train. Therefore, the intensity of the X shock can be adjusted upon the backpressure generated by combustion. Given the incoming flow properties and backpressure downstream, parameters at the exit of the X-shock model can be obtained from a set of oblique shock relations and the resulting parameters are compatible. Thus, the X-shock model has served to reflect the discontinuity caused by the shock train.

The combustion downstream is considered as quasi-1-D flow without shock, and a series of ODEs has been adopted. A uniformity process at the exit of X-shock control volume was taken to convert two-dimensional parameters into 1-D, which will be used as initials for the combustor ODEs. Additionally, the quasi-1-D method used in the present work employs an iterative procedure for the backpressure matching to simulate realistic phenomenon in the dual-mode combustor. That is, high pressure caused by the large amount of heat release in the combustor, propagating upstream through the boundary layer to the exit of the isolator, is matched by the pressure rise via the precombustion shock train.

Thus, the methodology in the present work employs the interactions between the combustor ODEs and solution of the X-shock model to reach a converged result. Currently, the present method can

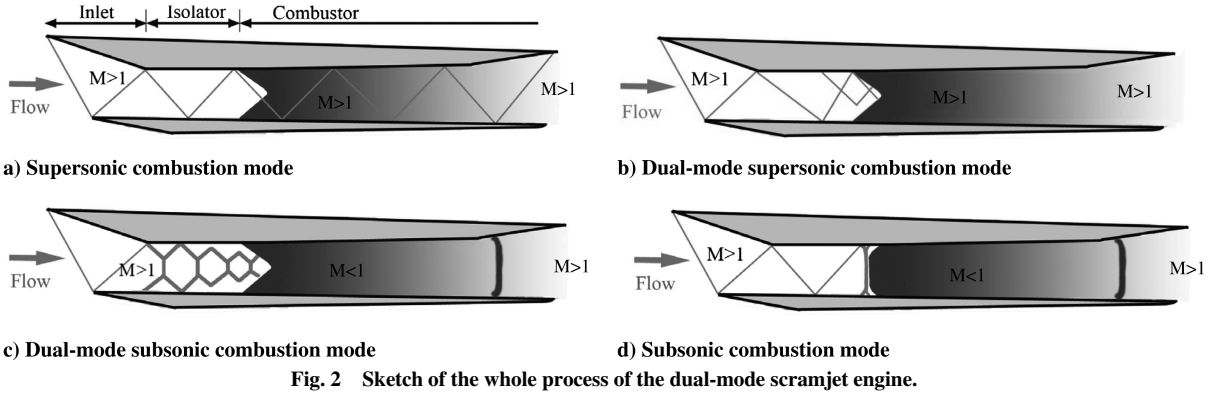

Fig. 2 Sketch of the whole process of the dual-mode scramjet engine.

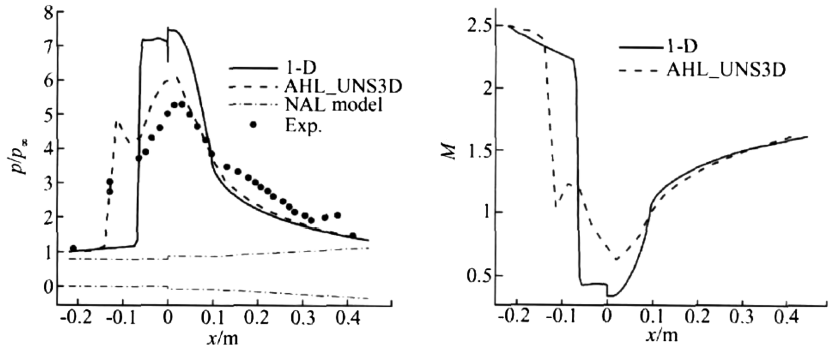

Fig. 3 Results of unsteady quasi-1-D model [13] (AHL_UNS3D-3D calculation in [13]; NAL-National Aerospace Laboratory of Japan).

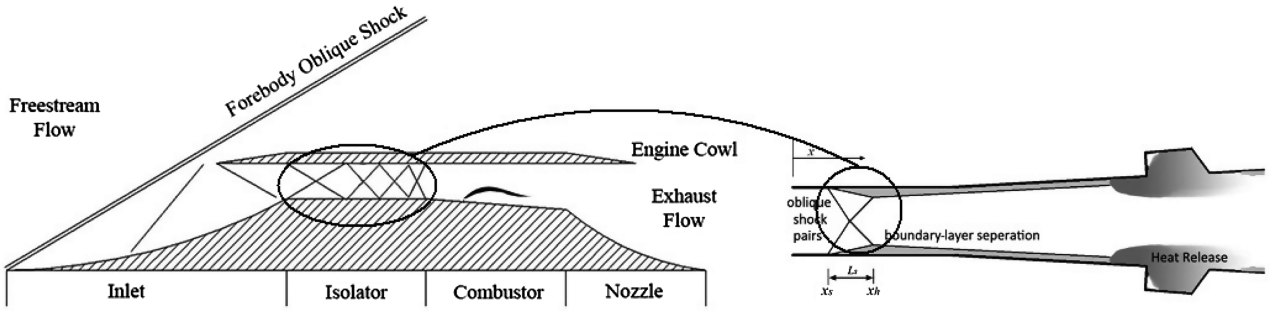

Fig. 4 Sketch of the dual-mode scramjet engine and X-shock model.

compute five different engine states (modes) in the dual-mode scramjet engine, which are 1) supersonic combustion mode, 2) dual-mode supersonic combustion mode, 3) dual-mode subsonic combustion mode, 4) subsonic combustion mode, and 5) inlet unstart.

In the following sections, the solution procedure will be described first. Then, the X-shock model and combustor model will be introduced, respectively. Some mathematical treatments will be mentioned in the last section.

A. Solution Procedure

A flowchart of the whole method is shown in Fig. 5, and the calculation can be briefly described in the following five steps:

1) First, assuming a "shock-free" state of the engine and giving the entry state of the isolator, all parameters along the duct from the inlet of the isolator to the outlet of the combustor are calculated by the ODEs. If the minimum Mach number chokes the flow, the X-shock model will be applied. Otherwise, the calculation is accomplished and combustion mode is supersonic combustion mode, in which very weak shock trains exist along the isolator and the pressure rise upstream of the injection can be nearly ignored.

2) If the X-shock model is needed according to the first step, a new iteration begins with its calculation based on the highest pressure obtained with the last step. The pressure rise ratio should be examined to ensure that it is lower than the maximum pressure rise ratio for a given inlet Mach number based on the normal shock relation: If the pressure rise ratio is larger than that of a normal shock, the normal shock would propagate upstream, causing the inlet unstart. The calculation stops.

3) If the pressure rise ratio is lower than that of a normal shock, the calculation of X shock starts. The length of precombustion shock should first be calculated. If the length of the shock train exceeds the

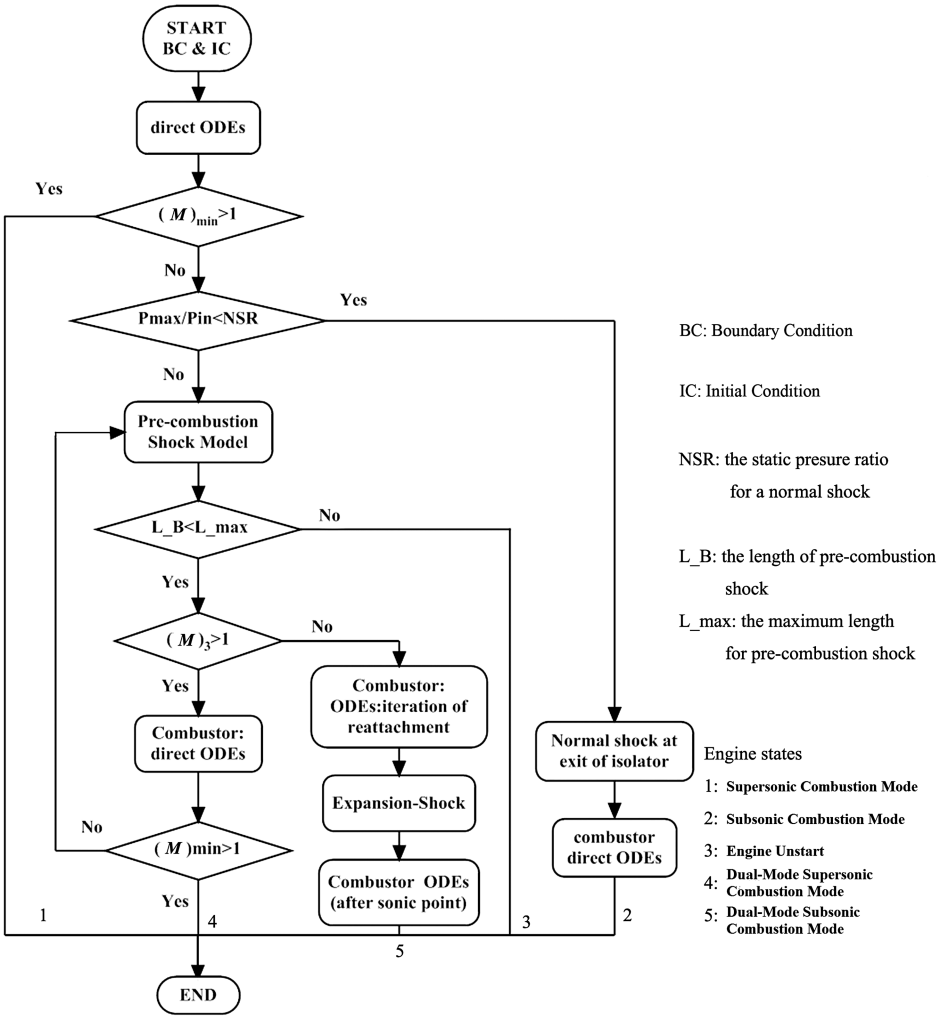

Fig. 5 Flowchart of the model.

maximum length of the isolator section upstream of the injection, the engine is also considered to unstart and the calculation terminates. Otherwise, we need to continue toward the fourth step.

4) Given incoming flow properties and high backpressure, parameters at the exit of the X-shock model can be obtained and averaged as initials for a new iteration of calculating ODEs. The iteration will be stopped after the solutions converge. Then, the state after the precombustion shock determines the engine state. That is, if the Mach number behind the precombustion shock train is larger than one, the engine works on dual-mode supersonic combustion mode.

5) If the Mach number after the X-shock model calculated in the fourth step is less than one, the engine mode is determined as the dual-mode subsonic combustion mode. In this mode, solution of the downstream flow uses an ad hoc method named "expansion-shock," as addressed in [14], to deal with singularity of the solution at sonic point.

Therefore, the present model can account for multimodes in the dual-mode scramjet engine.

B. Isolator Model

The isolator is very important because it is used to balance the pressure of the inlet and combustor through the shock train. The main characteristics are the intensity and length of the shock train. Therefore, the X-shock model was introduced to describe the strength of shock, and the semi-empirical equation was used for the length. Because the X-shock model is a two-dimensional model, an averaging process is required to connect with one-dimensional calculation in the combustor. Details will be mentioned in Secs. II.B.1 and II.B.2.

1. X-Shock Model

To represent the characteristics of precombustion shock, the X-shock model should include two basic features. First, it has to be strength adaptable and the pressure rise calculated by the X-shock model should account for that of the whole shock train. Then, as initials of 1-D combustor ODEs, the flow at the exit of the model should return in the streamwise direction.

Considering these demands, a novel precombustion shock model of an X-shaped shock was established, which includes two pairs of oblique shock with symmetry in the vertical direction, as shown in Fig. 6. Two oblique shocks caused by the boundary-layer separation intercept and reflect.

Assuming the same deflection angle, the main flow returns to the streamwise direction after the first and second shock. Given the inlet conditions and the peak pressure $P_{\max}$ caused by the combustion downstream, parameters of the shock region can be solved based on the conservation law of the control volume.

In the shock region, the thermodynamic parameters, such as constant-pressure specific heat and specific heat ratio, change with temperature. As shown in Fig. 6b, the aerodynamic parameters in the three regions of X shock are solved by equations of conversation laws and restrictive conditions, shown as follows, where the subscripts correspond to the region numbers depicted in Fig. 6b. Additionally, the flow is assumed to be adiabatic because there is no significant reaction and the heat loss through the wall can be almost neglected:

$$\rho_1 v_{1n} = \rho_2 v_{2n}, \quad \rho_1 v_{1n}^2 + p_1 = \rho_2 v_{2n}^2 + p_2, \quad v_{1t} = v_{2t},$$

$$h_1 + v_{1n}^2/2 = h_2 + v_{2n}^2/2 \quad \tan\beta_1 = v_{1n}/v_{1t},$$

$$\tan(\beta_1 - \theta_1) = v_{2n}/v_{2t}, \quad \sin\beta_1 = v_{1n}/v_1,$$

$$p_2 = \rho_2 R T_2 \quad h_2 = \int_{T_1}^{T_2} c_p \,\mathrm{d}T + h_1, \quad \rho_2 v_{2nn} = \rho_3 v_{3n},$$

$$\rho_2 v_{2nn}^2 + p_2 = \rho_3 v_{3n}^2 + p_3, \quad v_{2tt} = v_{3t} \quad h_2 + v_{2nn}^2/2 = h_3 + v_{3n}^2/2,$$

$$\tan\beta_2 = v_{2nn}/v_{2tt}, \quad \tan(\beta_2 - \theta_2) = v_{3n}/v_{3t},$$

$$\sin\beta_2 = v_{2nn}/v_2 \quad p_3 = \rho_3 R T_3, \quad h_3 = \int_{T_2}^{T} c_p \,\mathrm{d}T + h_2, \quad \theta_1 = \theta_2,$$

$$v_{2n}^2 + v_{2t}^2 = v_{2nn}^2 + v_{2tt}^2 = v_2^2$$

The intensity of the X shock stands for that of the shock train in the isolator, but the length of a reflected shock pair is much shorter. Thus, the length of the X shock should be extended to match that of the shock train. Billig proposed a semi-empirical equation for the length of shock train and modified coefficients according to experimental data of the rectangular isolator [15]. The empirical formula can be expressed as

$$\frac{L_s}{H} = \frac{\sqrt{(\theta/H)}}{\sqrt[4]{Re_\theta}} \cdot \frac{\{a[(p_{\max}/p_{\text{in}}) - 1] + b[(p_{\max}/p_{\text{in}}) - 1]^2\}}{(Ma_{\text{in}}^2 - 1)} \tag{1}$$

where the constants a and b are determined based on the experimental data. For the rectangular duct, a and b are 50 and 170, respectively. The Reynolds number Re_θ is obtained according to momentum thickness using the Prandtl analogy [16].

The oblique shock train accounts for the whole pressure rise before the injection. However, as indicated in previous works [17,18], normal shock trains usually propagate rather upstream and a mixing region exists between shock structure and combustion. Wall friction and area change would affect the static pressure in this region. For the constant-area isolator and diverging combustor adopted in [17,18] and the following experimental cases, the pressure rise caused by the normal shock train could only account for 80–90% of the maximum pressure before the injection (Fig. 7). Using the results from the present study, 90% of pressure rise is caused by the shock system, whereas the remaining 10% will be accomplished by 1-D calculation of friction and area diverging.

To sum up, the intensity of the X-shock model is solved by a series of conservation laws, whereas the length of the shock train is obtained through Eq. (1) with the given peak pressure after the shock system. When normal shock trains appear in the isolator, that is, the flow after the shock systems becomes subsonic, the area change and friction will play their parts in the section between shock trains and combustion. Particularly, 10% of pressure rise will be gained through the 1-D calculation of area change and friction before the combustion region.

2. Averaging Process

When the intensity and the length of the X-shock model is determined by the peak value of backpressure, solution of the ODEs

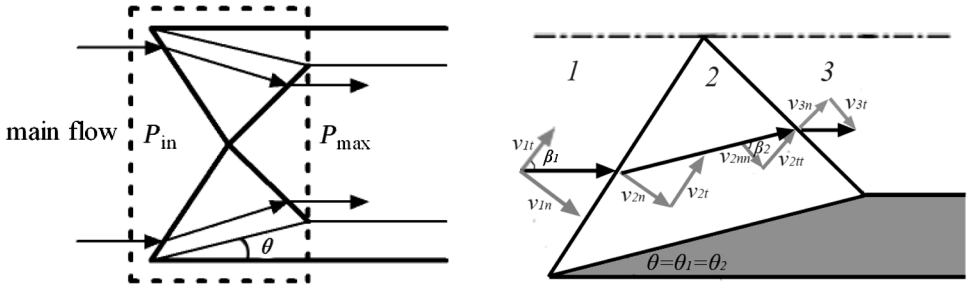

a) Control volume **b) Partial enlargement of control volume**

Fig. 6 Sketches of the X-shock model.

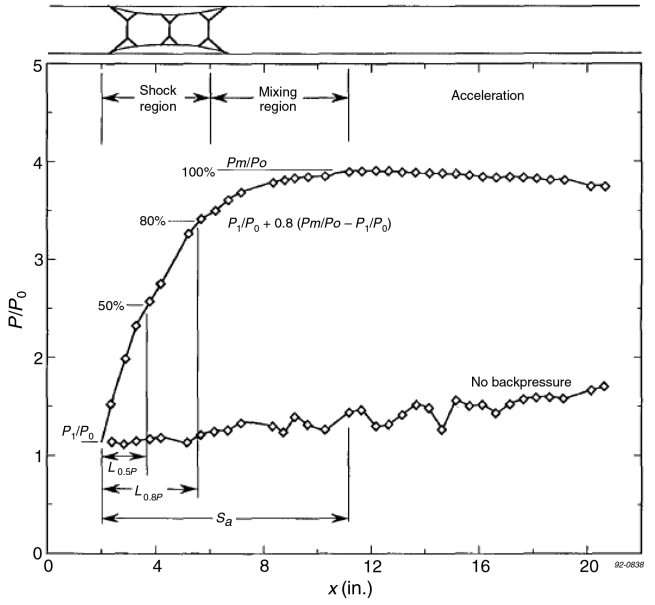

Fig. 7 Typical shock train pressure traces for $M = 2$ isolated entrance condition [17].

will begin and take parameters after the control volume of X shock as initials. However, the X shock is a two-dimensional model. As shown in Fig. 6a, the parameters in the core flow and in the separated region downstream of the shock structure are not the same, thus a process of averaging of flow parameters is needed (Fig. 8).

To guarantee the conservation of momentum, pressure is averaged by area weighting and velocity is averaged with a weight of mass flow rate. Through the conservation of mass, energy, and the equation of state, other aerodynamic parameters are obtained based on the averaged pressure and velocity. To connect the isolator and combustor calculations, an iterative process is used for ensuring that the averaged peak pressure outside the control volume (at the $u - u$ section) equals to the peak backpressure in the combustor.

To draw continuous distributions of aerodynamic parameters along the length of X shock, a cubic polynomial equation (2) has been adopted to link the inlet and obtain averaged parameters at the exit of the X shock:

$$\frac{\kappa(x)}{\kappa_i} = 1 + \left(\frac{\kappa_u}{\kappa_i} - 1\right)(3 - 2\chi)\chi^2, \qquad \chi \equiv \frac{x - x_i}{x_u - x_i} \tag{2}$$

where the subscripts i and u stand for the inlet and averaged parameters, respectively; x represents the streamwise position along the length of the X-shock model; and κ symbolizes all averaged parameters, including static pressure, static temperature, Mach number, total pressure, velocity, and density.

C. Combustor Model

As mentioned earlier, flow parameters of the combustor are calculated by a series of ODEs similar to that used in [9]. Equilibrium chemistry or "mixing-controlled" reaction is assumed for the energy source term.

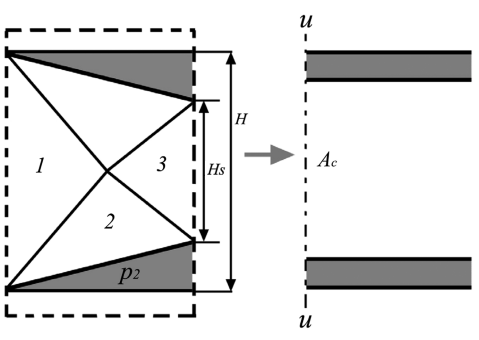

Fig. 8 Diagram of averaging process.

1. Governing Equations

The governing equations for the current analysis are based on the following assumptions: 1) quasi-one-dimensional flow (variables including area of the cross section are functions of the axial distance x only), 2) steady-state flow, and 3) the flow is assumed as perfect gas.

The conservations of mass, momentum, and energy are governed by the following equations:

$$\frac{1}{\dot{m}}\frac{\mathrm{d}\dot{m}}{\mathrm{d}x} = \frac{1}{\rho}\frac{\mathrm{d}\rho}{\mathrm{d}x} + \frac{1}{U}\frac{\mathrm{d}U}{\mathrm{d}x} + \frac{1}{A}\frac{\mathrm{d}A}{\mathrm{d}x} \tag{3}$$

$$\frac{1}{p}\frac{\mathrm{d}p}{\mathrm{d}x} + \gamma Ma^2\left(\frac{1}{U}\frac{\mathrm{d}U}{\mathrm{d}x} + \frac{2C_f}{D} + \frac{1}{\dot{m}}\frac{\mathrm{d}\dot{m}}{\mathrm{d}x}\right) = 0 \tag{4}$$

where the friction coefficient C_f is calculated by the empirical equation described by the Japan Aerospace Exploration Agency [19]. Besides, the coefficient of kinematic viscosity is obtained from Sutherland's law [20]. Only perpendicular injections will be discussed in the present study, thus the fuel injection momentum will not affect that in the x direction. Therefore, the conservation of momentum in the x direction can be expressed as Eq. (4).

$$\frac{1}{T}\frac{\mathrm{d}T}{\mathrm{d}x} + \frac{(\gamma - 1)Ma^2}{U}\frac{\mathrm{d}U}{\mathrm{d}x} - \left(1 + \frac{\gamma - 1}{2}Ma^2\right)\frac{\overline{C_{p0}}}{\overline{C_p}T_0}\frac{\mathrm{d}T_0}{\mathrm{d}x} = 0 \tag{5}$$

where $\overline{C_p}$ and $\overline{C_{p0}}$ represent the mean specific heat determined by static temperature and total temperature, respectively. They can be expressed in terms of the enthalpy of each species and obtained from a polynomial curve fit written in [21] according to the static temperature and species.

Additionally, for a perfect gas, the differential form of equation of state and Mach number can be written in terms of

$$\frac{1}{p}\frac{\mathrm{d}p}{\mathrm{d}x} = \frac{1}{\rho}\frac{\mathrm{d}\rho}{\mathrm{d}x} + \frac{1}{T}\frac{\mathrm{d}T}{\mathrm{d}x} - \frac{1}{\overline{MW}}\frac{\mathrm{d}\overline{MW}}{\mathrm{d}x} \tag{6}$$

where the mean mass molecular weight $\overline{MW}$ is a function of mass fraction and molecular weight for each species:

$$\frac{\mathrm{d}U}{U} = \frac{\mathrm{d}Ma}{Ma} + \frac{1}{2}\frac{\mathrm{d}T}{T} \tag{7}$$

In the present work, five parameters (p, T, M, ρ, and U) will be calculated by the ODEs. The ODEs, including Eqs. (3–7), are a stiff equation set. Thus, a stiff ODE solver should be provided. The solver used in this study is MATLAB ODE15s, which is based on the mechanism of the Gear algorithm [22]. The important aerodynamic parameters, total pressure, and entropy will be calculated using the integral formulas.

2. Combustion Model

A single-step global reaction model expressed as Eq. (8) is used for the evaluation of heat releasing of the equilibrium reaction assumption:

$$\varphi(\text{fuel}) + \text{Air} \rightarrow (1 - \eta_c)\varphi(\text{fuel}) + \text{products} \tag{8}$$

The fuel can be either hydrogen or hydrocarbon. The equivalence ratio φ and the combustion efficiency η_c affect the composition of the products, including O_2, N_2, H_2O, and CO_2. In this work, ethylene is taken as the fuel.

The heat release regions are assumed according to experimental data. As indicated by previous works, chemiluminescence is often used as a marker of the heat release rate in flames [23–26]. In hydrocarbon flames, we employ CH^* images to locate the heat

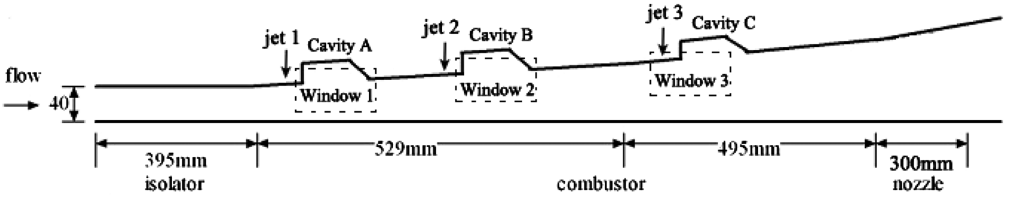

Fig. 9 Schematic of direct-connect scramjet test facility.

release distributions [27]. According to the experiments, uniform heat release has been adopted [7].

D. Mathematical Treatment

As a method to analyze different modes in the dual-mode scramjet engine, some mathematical treatments should be taken. Especially for dual-mode combustion modes, precombustion shock interacts with heat release downstream and the boundary-layer separation and reattachment. The treatment of the thermal throat is also crucial for the calculation stability.

In particular, the boundary layer is assumed to reattach at the end of heat release. The way of locating the thermal throat is similar to that in [28]. Here, expansion shock, that is, an inverse operation of the normal shock wave relationship, has been adopted at the thermal throat to ensure the stability of calculation.

III. Analysis of Direct-Connect Combustion Experiment

Comparisons with the dual-mode ethylene-fueled combustion experiments in the same configuration have been made to demonstrate the necessity to include an X-shock model and the ability of the present 1-D model to calculate different combustion modes.

The experiments used in this work were performed on the direct-connect combustor facility [29]. The test section is sketched in Fig. 9. The constant-area isolator with the cross section of 85×40 mm is followed with two diverging ducts with angles of 1.5 and 3.0 deg, respectively. Three parallel multiports ($7 \times \Phi 1.2$ mm) are located 60 mm upstream of the leading edge of wall cavities. The conditions of air flow and type of fuel injections are shown in Table 1.

Besides, the schlieren photos were taken at window 1 with a frame frequency of 10 kHz.

The quasi-one-dimensional method in the present work uses the same geometric area shown in Fig. 9 and entrance flow parameters measured in the experiments. Conditions of cases mentioned next are listed in Table 2. The area change caused by the cavities is neglected.

A. Comparison With One-Dimensional Model Without Shock Model

The original 1-D result based on the ODEs [7] set can usually agree well with the cases where the precombustion shock is so weak that pressure rise upstream of the injection can be almost ignored. However, when considerably more heat is added into the combustor, the minimum Mach number is not far from choking and precombustion shock will cause significant pressure rise. In this occasion, 1-D ODEs will meet the problems of singularity and also cannot agree with the pressure upstream due to the absence of shock model.

To illustrate the situation mentioned earlier, comparison has been made in the condition of case 1 listed in Table 2. The incoming air flow is at $M = 2.5$ and the equivalence ratio is 0.69.

Figure 10 compares the present 1-D numerical result to the original 1-D model without the X-shock model. The results of 1-D method without the X-shock model are drawn in dotted lines. The dashed lines represent the first step obtained from ODEs and solid lines show the convergent solutions of case 1 after iterations with the X-shock model. As shown in Fig. 10a, although the pressure comparison in the expansion section is somehow acceptable, the 1-D model without the X-shock model fails to predict the peak pressure limited by the singularity of ODEs (shown in Fig. 10b) and is not capable of obtaining the pressure rise caused by the precombustion shock. On the contrary, the present 1-D result with the X-shock model and iterative process agrees well with the experimental pressure data along the flowpath with an averaging error of approximately 9.2%. The peak pressure and its position show overpredictions of 1.6 and 9.8%, respectively. The propagation distance of the shock train upstream of the injection is also well predicted within 1.8% of the measured data. Considering the simplification of 1-D analysis and measurement errors in experiments, these errors are acceptable for analysis of different combustion modes and a preliminary design purpose.

Therefore, the present method can be applied to analyze dual-mode combustion. With the X-shock model, pressure rise is not only affected significantly by the heat release, but also relates to the effect of the shock train. The iterative process can reflect the flow mechanism between the precombustion shock and heat releasing downstream. The propagation of precombustion shock and the peak pressure can be better predicted. Without the X-shock model, the heat release could be overestimated when pure the ODEs set is employed to reach the peak pressure and even some impractical results can be obtained.

B. Analysis of Different Combustion Modes

To investigate the ability to analyze different combustion modes for the present 1-D method, analysis and comparison of three cases (cases 2–4) are conducted and their flow and fuel conditions are listed in Table 2. With $M = 2.5$, fuel injections of cases 2 and 3 are relatively separated, whereas case 4 has closer injections with $M = 1.8$.

1. Supersonic Combustion Mode

First, numerical results of case 2 listed in Table 2 have been compared with the corresponding experimental data. When the air flow Mach number is relatively high and the fuel equivalence ratio is comparatively low in the combustor, only weak shock structures appear in the isolator and the pressure rise upstream of the fuel injection will not be significantly affected.

Figure 11 illustrates the pressure and Mach number distributions of case 2. In the calculation, the lowest Mach number obtained in the first step is above one and iteration with the isolator has not been used. Moreover, it can be seen that the predicted pressure agrees well with the experimental one within an overall averaging error of 9.3%. The peak pressure and position are also well predicted. The pressure rising position overpredicted by 5.4% is located right after the injection, which indicates that there is no strong precombustion shock upstream in the isolator. As clarified in the Introduction, this engine state is called supersonic combustion mode.

Table 1 Experimental conditions for current study

Mach no.	Total temperature, K	Total pressure, MPa	Mass flow rate, kg/s	Fuel
1.8	1000	0.56	1.2	Ethylene
2.5	1500	1	1.6	Ethylene

Table 2 Conditions of cases for experiment and 1-D model

No.	Injections	Equivalence ratio	M_{in}	$T_{0,in}$, K	$\dot{m}_{in}$, kg/s
1	Jet 1, jet 3	0.69	2.5	1500	1.2
2	Jet 1, jet 3	0.38	2.5	1500	1.2
3	Jet 1, jet 3	0.52	2.5	1500	1.2
4	Jet 2, jet 3	0.56	1.8	1000	1.6

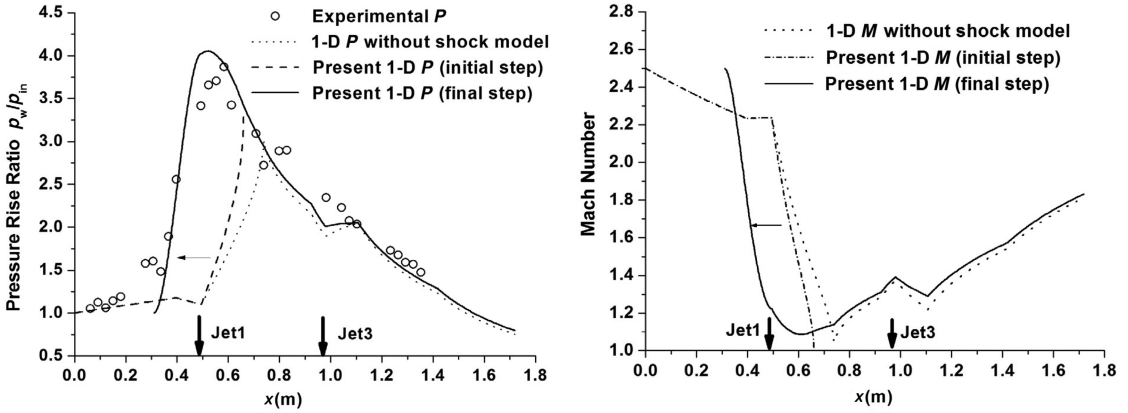

a) Nondimensional static pressure b) Mach number

Fig. 10 Axial distributions for case 1.

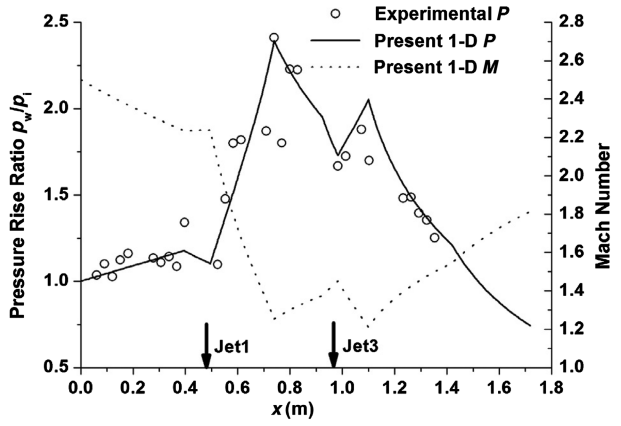

Fig. 11 Nondimensional pressure and Mach number distribution for case 2.

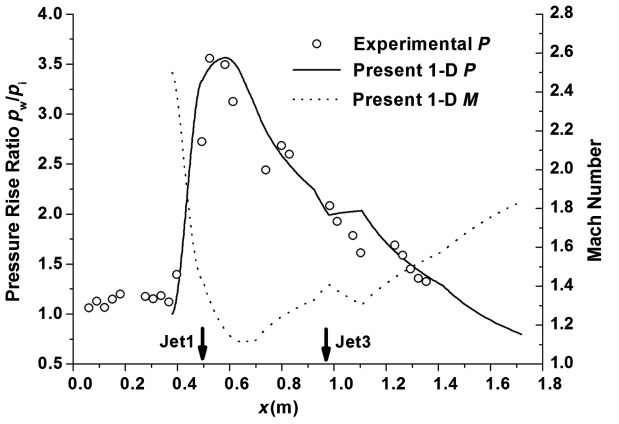

Fig. 13 Nondimensional pressure and Mach number distribution for case 3.

2. Dual-Mode Supersonic Combustion Mode

When the fuel equivalence ratio rises in the combustor, higher pressure caused by the intense combustion could generate pre-combustion shock train upstream.

This phenomenon can be observed in the dual-mode combustor of case 3 shown in Fig. 12. A series of schlieren photographs shows the formation of precombustion shock and its propagation. Combustion first occurs at the rear of wall cavity, then the flame diffuses in the whole cavity. The pressure rise due to the combustion generates shock upstream of the cavity. The last three photos show that the heat releasing forces the shock to propagate upstream until it cannot be observed in the window.

Figure 13 compares the present 1-D numerical result to experimental data of case 3. Good agreement of static pressure is seen along the whole engine path with an averaging error of 9.8%. The resulting error in peak pressure value is an underprediction of 2.1%, whereas that in peak pressure position is 10.5% behind the experimental data. The crucial propagation distance of the shock train ahead of the

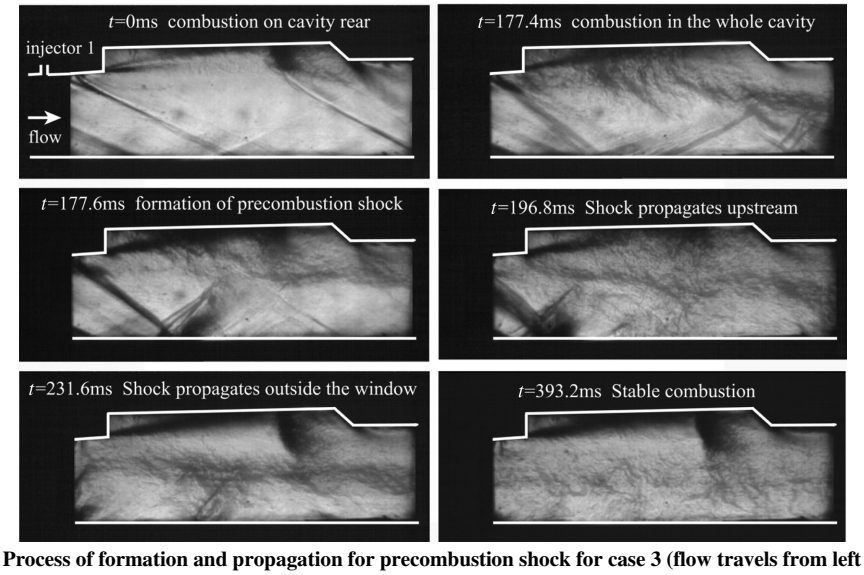

Fig. 12 Process of formation and propagation for precombustion shock for case 3 (flow travels from left to right).

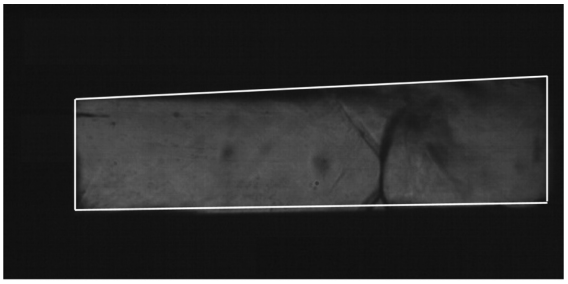

Fig. 14 Schlieren photo of precombustion shock for case 4 (window 1) (flow travels from left to right).

injection is well predicted within 5.0% of the measured data. According to the solid line in Fig. 13, the averaged Mach number along the engine duct is above one. Furthermore, the tunable diode laser absorption spectrum (TDLAS) [30] was implemented at the isolator ($x = 0.2$ in Fig. 13), combustor ($x = 0.8$), and nozzle ($x = 1.54$). The resulting averaging Mach numbers of TDLAS calculated by measured temperature and velocity are 2.42, 1.28, and 1.83, respectively. The isolator data validate the experimental inlet condition, whereas the latter two values agree well that of 1.26 and 1.71 in Fig. 13. The overall agreement validates our assumptive state of case 3 and verifies that the present method can also be applied to analyze the dual-mode supersonic combustion mode.

3. Dual-Mode Subsonic Combustion Mode

A normal shock train was observed in the experimental schlieren photo of case 4 shown in Fig. 14. Referring to Table 2, the injection of case 4 begins around window 2, but the normal shock train propagates to window 1. This phenomenon indicates that a large amount of heat release should exist and subsonic combustion occurs in the combustor.

By applying the quasi-1-D method to case 4, distributions of aerodynamic parameters can be obtained. The comparison of pressure between numerical and experimental data is quite satisfactory with an averaging error of 9.5%. Both peak pressure value and position have been well predicted with errors of 6.6 and 1.9%, respectively. The propagation of precombustion shock can be accurately predicted, as shown in Fig. 15. Additionally, the calculated Mach number results ($M = 0.76$ at $x = 0.8$, $M = 1.63$ at $x = 1.54$) coincide with the TDLAS results both in the combustor ($M = 0.70$ at $x = 0.8$) and nozzle ($M = 1.50$ at $x = 1.54$). Good agreement proves the engine state to be the dual-mode subsonic combustion mode, as indicated by the Mach number distribution in Fig. 15.

If the precombustion shock propagates upstream of isolator entrance, the quasi-1-D can detect "engine unstart" and stops the calculation. To sum up, the quasi-1-D method presented earlier can analyze multimodes in a dual-mode combustor.

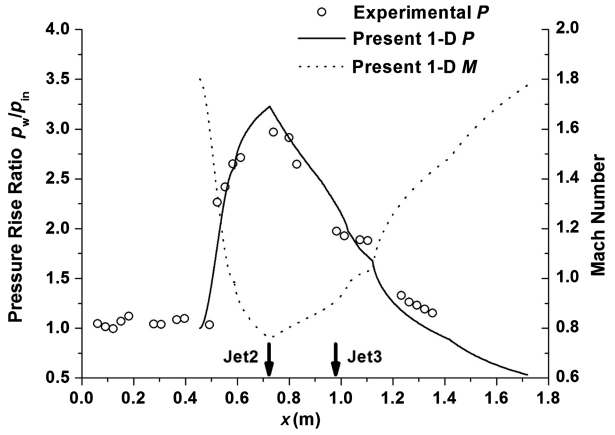

Fig. 15 Nondimensional pressure and Mach number distribution for case 4.

IV. Conclusions

A quasi-one-dimensional method with iterations considering the propagation of precombustion shock has been discussed and a novel precombustion shock model was proposed for establishing a strength-adaptable shock model in the isolator. Analysis has been made to compare the current method with diverse experimental data obtained from a dual-mode combustor. The results show that the present method can predict flow properties quite well for different modes that might occur in the dual-mode scramjet engine.

Furthermore, an accurate modeling of the precombustion flow region ensures a better understanding of pressure rise caused by shock train and combustion and then a more precise estimation of the engine thrust. Thus, this efficient method can be further implemented for the optimization of a dual-mode scramjet. The accurate prediction of engine performance would facilitate the engine design.

Acknowledgment

This research is supported by National Natural Science Foundation of China (11002148).

References

[1] McClinton, C. R., Rausch, V. L., Nguyen, L. T., and Sitz, J. R., "Preliminary X-43 Flight Test Results," *Acta Astronautica*, Vol. 57, Nos. 2–8, 2005, pp. 266–276. doi:10.1016/j.actaastro.2005.03.060

[2] Smart, M. K., Hass, N. E., and Paull, A., "Flight Data Analysis of the HyShot 2 Scramjet Flight Experiment," *AIAA Journal*, Vol. 44, No. 10, 2006, pp. 2366–2375. doi:10.2514/1.20661

[3] Billig, F. S., "Design of Supersonic Combustors Based on Pressure-Area Fields," *Symposium (International) on Combustion*, Vol. 11, No. 1, 1967, pp. 755–769.

[4] Daines, R., and Segal, C., "Combined Rocket and Airbreathing Propulsion Systems for Space-launch Applications," *Journal of Propulsion and Power*, Vol. 14, No. 5, 1998, pp. 605–612. doi:10.2514/2.5352

[5] Curran, E. T., Heiser, W. H., and Pratt, D. T., "Fluid Phenomena in Scramjet Combustion Systems," *Annual Review of Fluid Mechanics*, Vol. 28, No. 1, 1996, pp. 323–360. doi:10.1146/annurev.fl.28.010196.001543

[6] Chang, P., and Yu, G., "Study of One-Dimensional Flow Analysis Model of the Combustor in Supersonic Combustion Experiments," *Experiments and Measurements in Fluid Mechanics*, Vol. 17, No. 1, 2003, pp. 88–92 (in Chinese).

[7] Chen, Q., Chen, L. H., Gu, H. B., and Chang, X. Y., "Investigation of the Effect and Optimization of Heat Release Distributions in the Combustor on Scramjet Performance," *Journal of Propulsion Technology*, Vol. 30, No. 2, 2009, pp. 135–138 (in Chinese).

[8] O'Brien, T., Starkey, R., and Lewis, M., "Quasi-One-Dimensional High-Speed Engine Model with Finite-Rate Chemistry," *Journal of Propulsion and Power*, Vol. 17, No. 6, 2001, pp. 1366–1374. doi:10.2514/2.5889

[9] Birzer, C., and Doolan, C., "Quasi-One-Dimensional Model of Hydrogen-Fueled Scramjet Combustors," *Journal of Propulsion and Power*, Vol. 25, No. 6, 2009, pp. 1220–1225. doi:10.2514/1.43716

[10] Bussing, T. R. A., and Murman, E. M., "One-dimensional Unsteady Model of Dual-Mode Scramjet Operation," AIAA Paper 1983-0422, 1983.

[11] Ma., F., Li, J., Yang, V., Lin, K., and Jackson, T., "Thermoacoustic Flow Instability in a Scramjet Combustor," *41st AIAA/ASME/SAE/ASEE Joint Propulsion Conference & Exhibit*, AIAA Paper 2005-3824, 2005. doi:10.2514/6.2005-3824

[12] Lockwood, M. K., Petley, D. H., Martin, J. G., and Hunt, J. L., "Airbreathing Hypersonic Vehicle Design and Analysis Methods and Interactions," *Progress in Aerospace Sciences*, Vol. 35, No. 1, 1999, pp. 1–32. doi:10.1016/S0376-0421(98)00008-6

[13] Wang, L., Xing, J. W., Zheng, Z. H., Le, J. L., and Sutherland, W., "One Dimensional Evaluation of the Scramjet Flowpath Performance," *Journal of Propulsion Technology*, Vol. 29, No. 6, 2008, pp. 641–645 (in Chinese).

[14] Torrez, S., Driscoll, J., Ihme, M., and Fotia, M., "Reduced-Order Modeling of Turbulent Reacting Flows with Application to Ramjets and

Scramjets," *Journal of Propulsion and Power*, Vol. 27, No. 2, 2011, pp. 371–382.
doi:10.2514/1.50272

[15] Billig, F., "Research on Supersonic Combustion," *Journal of Propulsion and Power*, Vol. 9, No. 4, 1993, pp. 499–514.
doi:10.2514/3.23652

[16] White, F. M., *Viscous Fluid Flow*, 2nd ed., McGraw–Hill, New York, 1991, pp. 429–430.

[17] Sulins, G., and McLafferty, L., "Experimental Results of Shock Trains in Rectangular Ducts," *AIAA 4th International Aerospace Planes Conference*, AIAA Paper 92-5103, 1992.

[18] Tu, Q., and Seal, C., "Isolator/Combustion Chamber Interactions During Supersonic Combustion," *45th AIAA/ASME/SAE/ASEE Joint Propulsion Conference & Exhibit*, AIAA Paper 2009-4845, 2009.

[19] Mitani, T., Hirawa, T., Tarukawa, Y., and Masuya, G., "Drag and Total Pressure Distributions in Scramjet Engines at Mach 8 Flight," *Journal of Propulsion and Power*, Vol. 18, No. 4, 2002, pp. 953–960.
doi:10.2514/2.6022

[20] Sutherland, W., "The Viscosity of Gases and Molecular Force," *Philosophical Magazine*, Vol. 5, No. 36, 1893, pp. 507–531.
doi:10.1080/14786449308620508

[21] Burcat, A., and Ruscic, B."Third Millennium Ideal Gas and Condensed Phase Thermochemical Database for Combustion," Technion Aerospace Engineering Rept. 960, Lemont, IL, 2005.

[22] MATLAB, Software Package, Ver. R2010a, The MathWorks, Natick, MA, 2010.

[23] Price, R. B., Hule, I. R., and Sugden, T. M., "Optical Studies of the Generation of Noise in Turbulent Fames," *Proceedings of the Combustion Institute*, Vol. 12, No. 1, 1969, pp. 1093–1102.
doi:10.1016/S0082-0784(69)80487-X

[24] Najm, H. N., Paul, P. H., Mueller, C. J., and Wycokoff, P. S., "On the Adequacy of Certain Experimental Observables as Measurements of Flame Burning Rate," *Combustion and Flame*, Vol. 113, No. 3, 1998, pp. 312–332.
doi:10.1016/S0010-2180(97)00209-5

[25] Hardalupas, Y., and Orain, M., "Local Measurements of the Time-Dependent Heat Release Rate and Equivalence Ratio Using Chemiluminescent Emmission from a Flame," *Combustion and Flame*, Vol. 139, No. 3, 2004, pp. 188–207.
doi:10.1016/j.combustflame.2004.08.003

[26] Meier, W., Weigand, P., Duan, X. R., and Giezendanner-Thoben, R., "Detailed Characterization of the Dynamics of Thermoacoustic Pulsations in a Lean Premixed Swirl Flame," *Combustion and Flame*, Vol. 150, Nos. 1–2, 2007, pp. 2–26.
doi:10.1016/j.combustflame.2007.04.002

[27] Tian, L., Chen, L. H., Chen, Q., Li, F., and Chang, X. Y., "Modeling and Measurements of Heat Release Distributions in Dual-Mode Scramjet Combustor," *18th AIAA/3AF International Space Planes and Hypersonic Systems and Technologies Conference*, AIAA Paper 2012-5833, 2012.

[28] Torrez, S. M., Dalle, D. J., and Driscoll, J. F., "New Method for Computing Performance of Choked Reacting Flows and Ramto-Scram Transition," *Journal of Propulsion and Power*, Vol. 29, No. 2, 2013, pp. 433–445.
doi:10.2514/1.B34496

[29] Wei, Z., Chen, L. H., Chang, X. Y., Gu, H. B., and Li, F., "Performance of the Fuel Injector in Supersonic Combustor," *16th AIAA/DLR/DGLR International Space Planes and Hypersonic Systems and Technologies Conference*, AIAA Paper 2009-7250, 2009.

[30] Li, F., Yu, X. L., Gu, H. B., Li, Z., Zhao, Y., Ma, L., Chen, L., and Chang, X., "Simultaneous Measurements of Multiple Flow Parameters for Scramjet Characterization Using Tunable Diode-Laser Sensors," *Applied Optics*, Vol. 50, No. 36, 2011, pp. 6697–6707.
doi:10.1364/AO.50.006697

R. Bowersox
Associate Editor